Seismicity Properties of the Chain Transform Fault Inferred from OBS Data Obtained from the PI-LAB Experiment

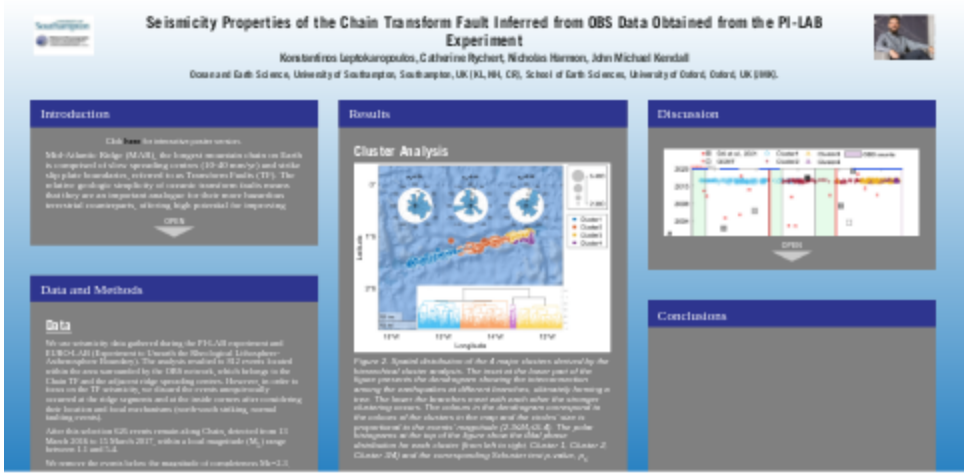

This website uses cookies to ensure you get the best experience on our website. Learn more
Accept

Konstantinos Leptokaropoulos, Catherine Rychert, Nicholas Harmon, John Michael Kendall

Ocean and Earth Science, University of Southampton, Southampton, UK [KL, NH, CR], School of Earth Sciences, University of Oxford, Oxford, UK [JMK].

PRESENTED AT:

INTRODUCTION

Click **here** (https://agu2021fallmeeting-agu.ipostersessions.com/default.aspx?s=AB-68-F1-E7-5D-55-84-8F-F2-20-51-E2-D5-F4-F3-95&guestview=true)for interactive poster version.

Mid-Atlantic Ridge (MAR), the longest mountain chain on Earth is comprised of slow spreading centres (10-40 mm/yr) and strike slip plate boundaries, referred to as Transform Faults (TF). The relative geologic simplicity of oceanic transform faults means that they are an important analogue for their more hazardous terrestrial counterparts, offering high potential for improving insights into the earthquake cycle. However, It is likely that oceanic lithosphere demonstrates significant mechanical anisotropies, with closely spaced faults, dikes and other features created during seafloor spreading in MAR.

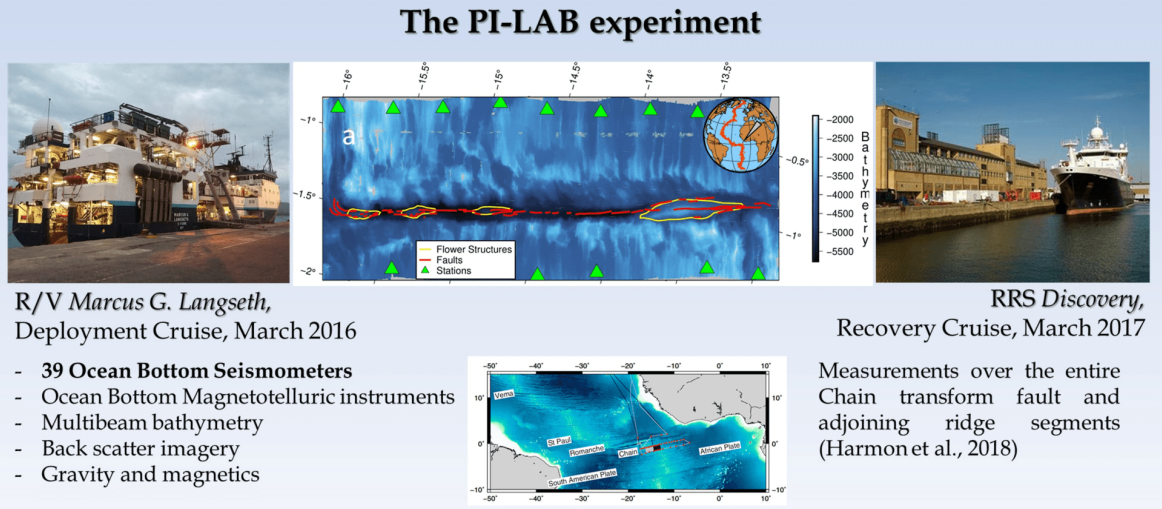

Figure 1. Study area and PI-LAB experiment overview

We combine microseismicity and geophysical data (bathymetry, tidal height, gravity anomalies) obtained under the PI-LAB experiment (Passive Imaging of the Lithosphere-Asthenosphere Boundary, Harmon et al., 2018) to evaluate the seismotectonic properties along Chain TF, an over 300 km long Transform Fault in the equatorial Mid-Atlantic Ridge.

Acknowledgements

PI-LAB, Natural Environment Research Council (NE/M003507/1)

EURO-LAB, European Research Council (GA 638665)

DATA AND METHODS

Data

We use seismicity data gathered during the PI-LAB experiment and EURO-LAB (Experiment to Unearth the Rheological Lithosphere-Asthenosphere Boundary).

The location of the events is performed by NonLinLoc software (Lomax et al., 2000). The analysis resulted to 812 events located within the area surrounded by the OBS network, which belongs to the Chain TF and the adjacent ridge spreading centres. However, in order to focus on the TF seismicity, we discard the events unequivocally occurred at the ridge segments and at the inside corners after considering their location and focal mechanisms (north-south striking, normal faulting events).

After this selection 626 events remain along Chain, detected from 13 March 2016 to 15 March 2017, within a local magnitude (M_L) range between 1.1 and 5.4.

We remove the events below the magnitude of completeness Mc=2.3, resulting to a dataset of 370 events along the transform valley, which are used for the analysis.

The hypocentre depths as well as focal mechanisms of well-recorded events are calculated by Grond software (Heimann et al., 2018 (https://agupubs.onlinelibrary.wiley.com/doi/10.1029/2021JB022251#jgrb55139-bib-0032)) using a Bayesian-bootstrap time-domain deviatoric moment tensor inversion.

In order to extend our analysis back in time by considering stronger earthquakes (M_W>~5.0) from Global Centroid Moment Tensor (GCMT) since 1977 (Ekström et al., 2012) and relocated strong events (M_W>5.5) since 1990 (Shi et al., 2021).

The geophysical data (Mantle Bouguer Anomaly - MBA, residual Mantle Bouguer Anomaly - rMBA and bathymetry) were taken from Harmon et al. (2018).

Methods

- The completeness magnitude, M_C, is estimated by the Anderson-Darling (AD) test (Marsaglia and Marsaglia, 2004; Leptokaropoulos, 2020).

- The Maximum likelihood estimation of b-value is applied (Aki, 1965). However, since we encounter significant b-value fluctuations as a function of magnitude cut-off, typical for small datasets (e.g. Leptokaropoulos et al., 2018), we further apply the repeated median technique (Siegel, 1982; Amorèse et al., 2010), which is highly resistant to observational uncertainties and outliers providing more robust results for small data sets. The significance of the b-value difference was evaluated by a bootstrap t-test (Amorèse et al., 2010).

- The stress inversion algorithm of Michael (1984), modified by Vavrycuk (2014) is applied to derive the orientation and relative amplitude of principal stresses from focal mechanisms.

- Multi-dimensional cluster analysis is performed by Ward (1963) hierarchical clustering technique, which creates subsequent branches of interconnection among earthquakes. Several earthquake (longitude, latitude, M_L) and geophysical (Tidal height, MBA, rMBA and bathymetry) parameters are used, demonstrating different scaling and distribution.

For this reason, before committing cluster analysis, we first transform all the aforementioned parameters into their equivalent dimensions (Lasocki, 2014).

- The SPOTL software (Agnew, 1997) is used to calculate solid Earth tides as well as ocean loading with the global ocean tide model TPXO72.2010 (Egbert & Erofeeva, 2002). The tidal phase is defined relative to low tides (Leptokaropoulos et al. 2021; *ϕ=0, low tide; ϕ=-180 and 180, the previous and subsequent high tides, respectively)*, and the Schuster (1897) test is applied to quantify the randomness of seismic events' occurrence time distribution.
- The Coulomb software package (Toda et al., 2005; Lin and Stein, 2004) is used to calculate Coulomb failure function variations (ΔCFF).

RESULTS

Cluster Analysis

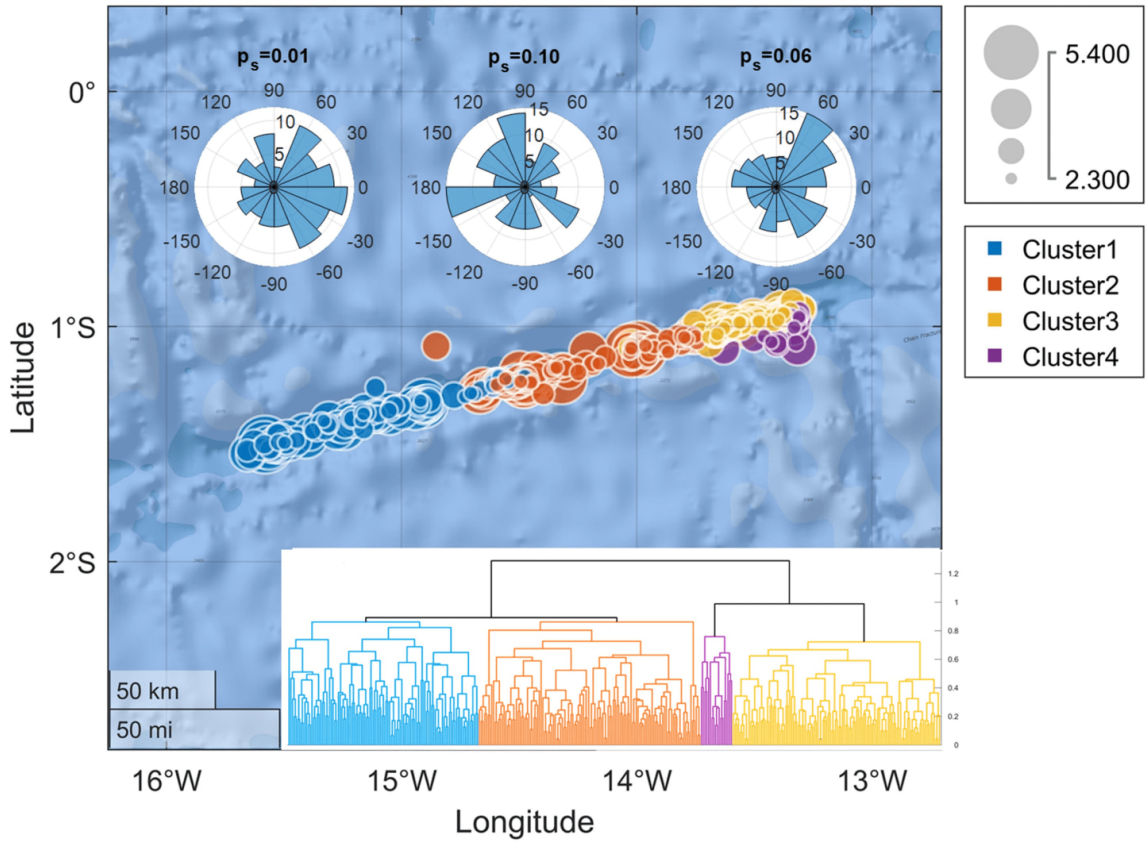

Figure 2. Spatial distribution of the 4 major clusters derived by the hierarchical cluster analysis. The inset at the lower part of the figure presents the dendrogram showing the interconnection among the earthquakes at different branches, ultimately forming a tree. The lower the branches meet with each other the stronger clustering occurs. The colours in the dendrogram correspond to the colours of the clusters in the map and the circles' size is proportional to the events' magnitude ($2.3 \leq M_L \leq 5.4$). The polar histograms at the top of the figure show the tidal phase distribution for each cluster (from left to right, Cluster 1, Cluster 2, Cluster 3/4) and the corresponding Schuster test p-value, p_s.

Magnitude Distribution

[VIDEO] https://res.cloudinary.com/amuze-interactive/video/upload/vc_auto/v1637316330/agu-fm2021/AB-68-F1-E7-5D-55-84-8F-F2-20-51-E2-D5-F4-F3-95/Video/b-values_rvnpyt.mp4

Figure 3. Along-strike magnitude distribution in Chain TF, considering different event windows from 50 to 100 events, overlapping by 1 event. Each calculation is shown as a coloured circle, centred at the longitude of the central event in each window.

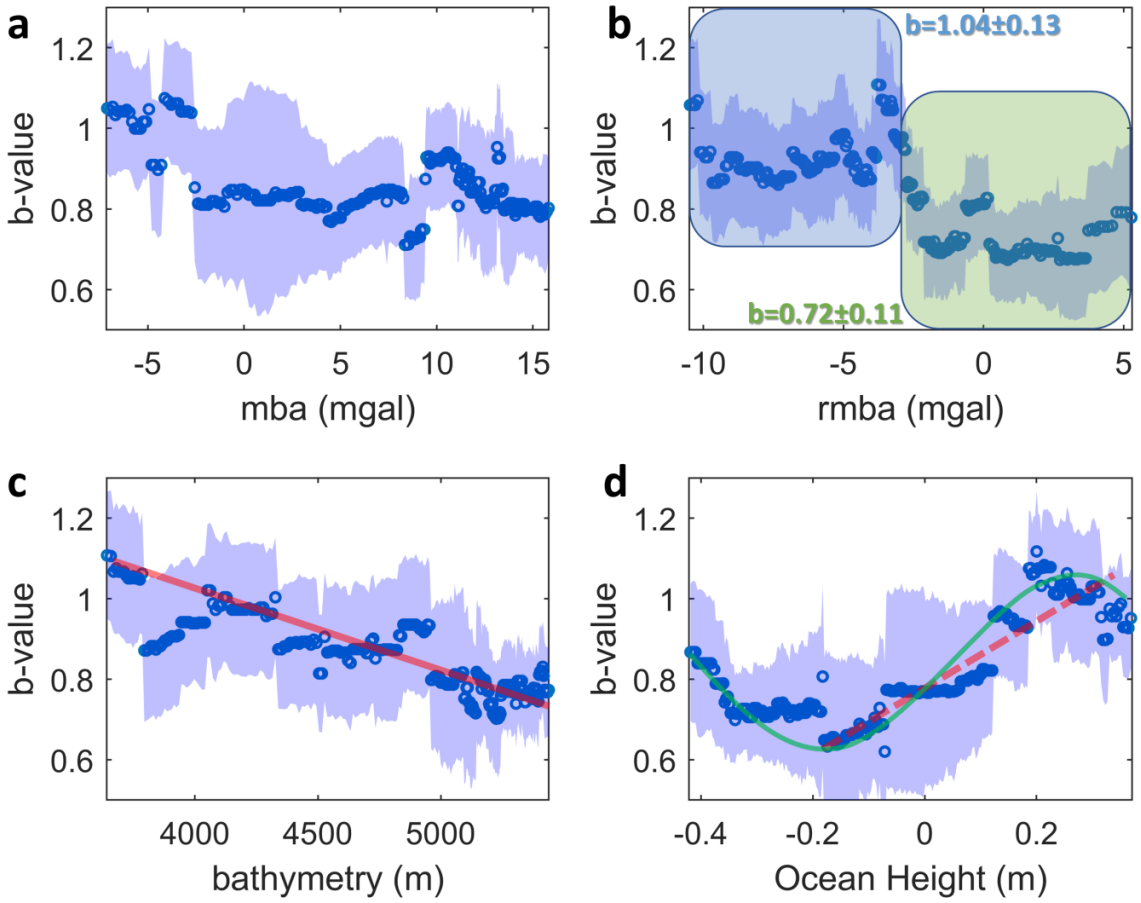

Figure 4. Single-parameter influence on magnitude distribution: (a) MBA (mgal), (b) rMBA (mgal), (c) bathymetry (m) and (d) ocean height (m). The blue dots show the b-value estimated by the repeated median technique for 100-event windows, plotted in the centre of each window. The windows are shifted by 1 event after each calculation. The shaded areas show the bootstrap standard error of b-value estimation, derived by 1,000 resamplings. The red lines show average linear trends, whereas the green line in (d) indicates a sinusoidal approximation with peaks at approximately ±0.20 m.

Coulomb Stress Changes

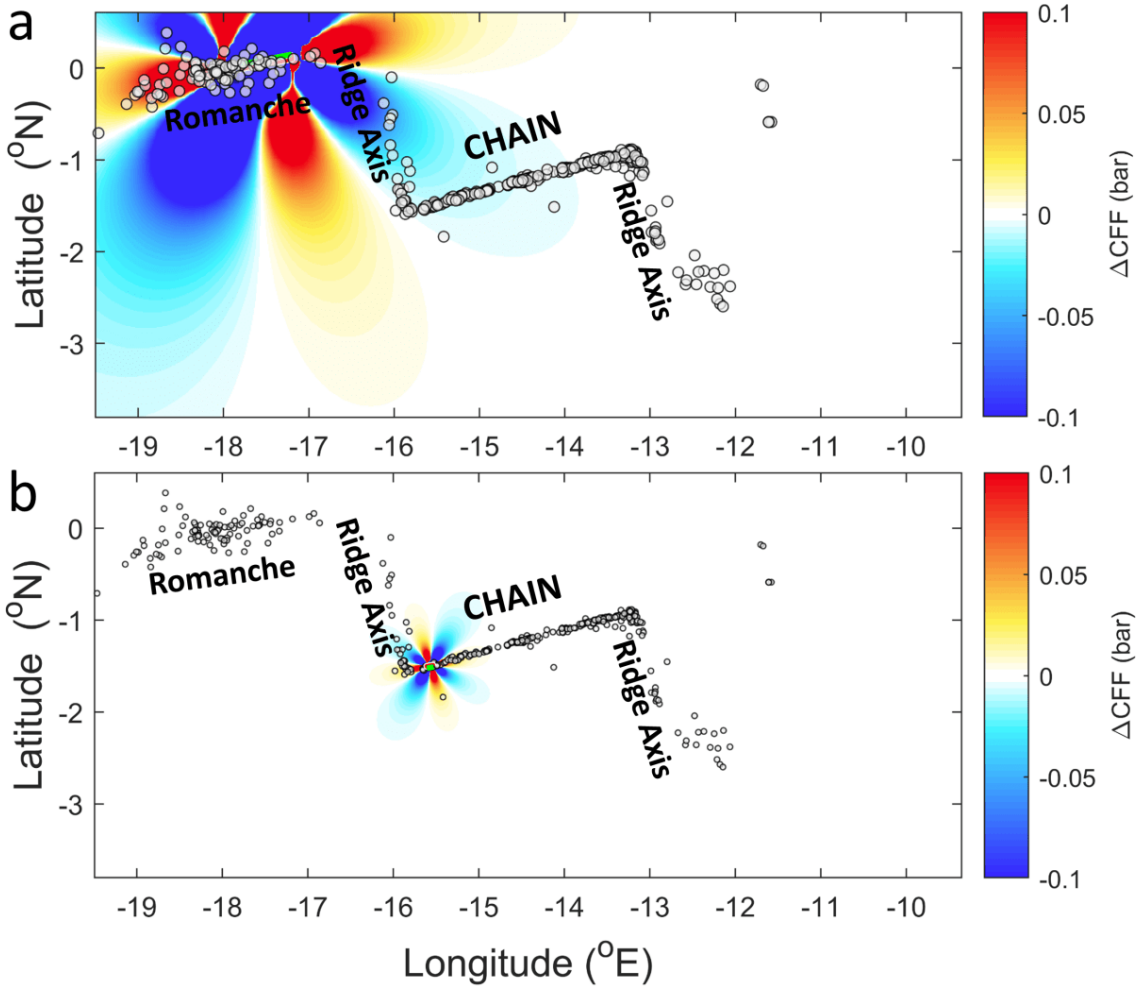

Figure 5. ΔCFF variation caused by a) the M_W7.1 event (Romanche TF) and b) the M_L=5.4 event (Chain TF). Warm colors represent positive ΔCFF whereas cold colors correspond to negative ΔCFF. The circles indicate the epicentres of earthquakes with M_L≥2.3 occurred across the two transform systems and the adjacent ridge spreading centres during the operation of the PI-LAB network. The map boundaries and color scales are identical for comparison. We investigated the possibility of influence of seismicity from remote 15 remote events during the network operation, based on seismicity rate changes along Chain. We found no evidence for potential dynamic triggering.

Stress Inversion

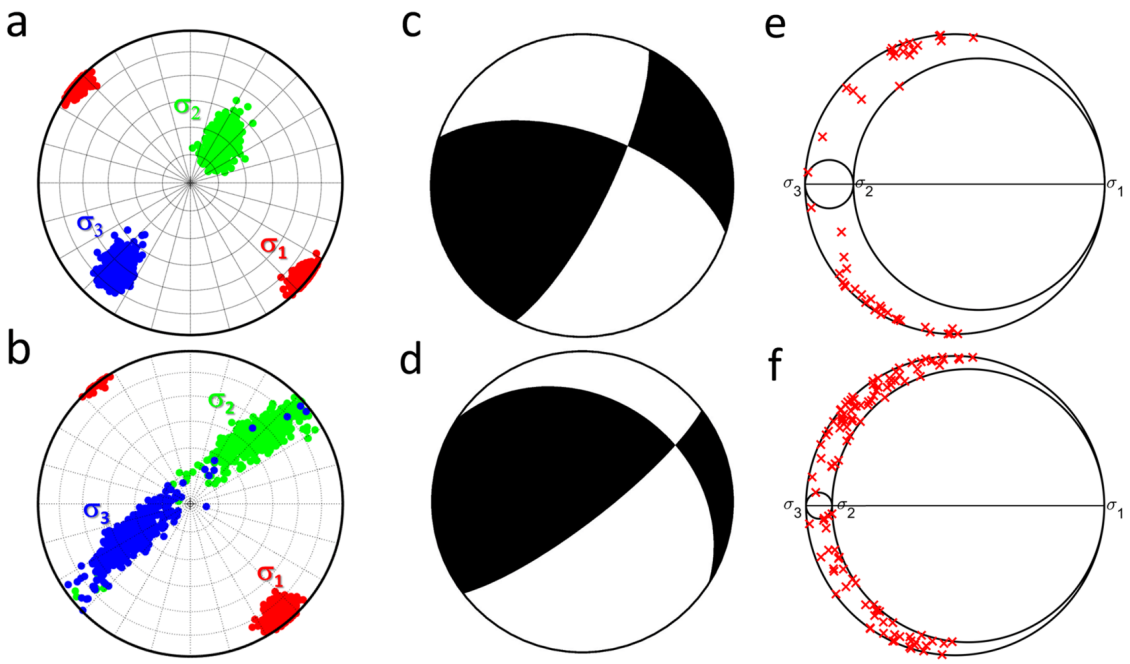

Figure 6. Confidence intervals of the principal stresses orientation, for (47) Q1-Q2 mechanisms (a) and all (112) mechanisms (b). Principal focal mechanism, shown as lower hemisphere projection, with compression denoted by black, for Q1-Q2 mechanisms (c) and all 112 mechanisms (d). Mohr's circle plot showing the relative magnitudes of the principal stresses, with the positions of the faults indicated by red crosses, for Q1-Q2 mechanisms (e) and all 112 mechanisms (f). The shape ratio is R=0.84 and R=0.91 for the 47 and 112 mechanisms, respectively.

DISCUSSION

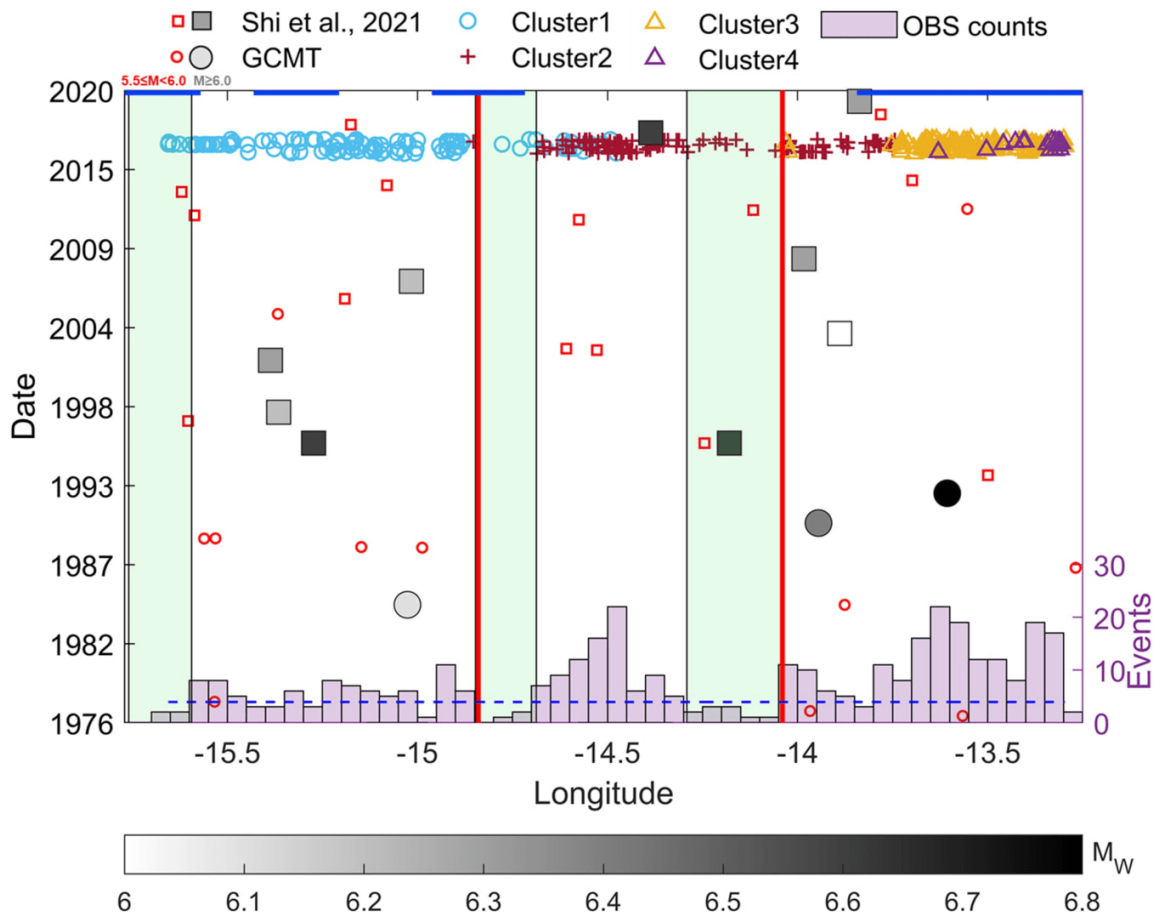

Figure 7. Longitude-date scheme, integrating the data and results from microseismicity (OBS) analysis, global CMT (circles) and Shi et al. (2021) relocated data (squares). The 4 Clusters in which OBS data were grouped by our cluster analysis are shown at the top of the plot, near Date=2016, by various symbols (see legend for details). The histogram at the bottom of the plot shows the number of microseismicity events per 0.05° longitude bins. The horizontal dashed line equals to a seismicity level ~8 events, corresponding to half the average rate per 0.05° longitude units. We define seismicity gaps when the rate falls below this level for more than 3 longitude bins. Based on this definition, 3 characteristic seismic gaps are identified, depicted by the green shaded bars. The red vertical lines divide Chain TF into three segments delineated by the seismic gaps. The blue horizontal lines just below the legend indicate the location of the flower structures.

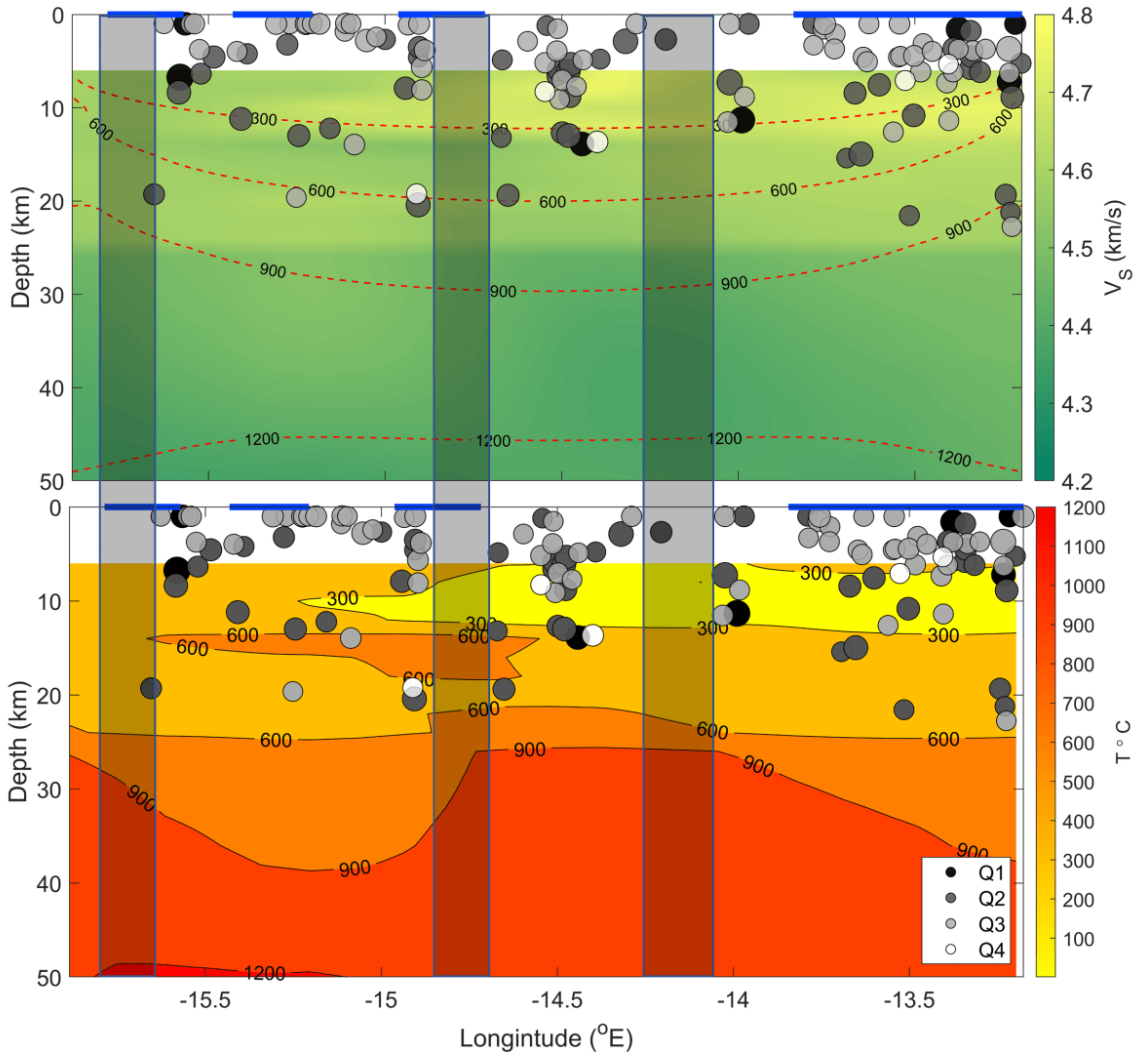

Figure 8. Cross section of Chain TF. a) Vertical distribution of the 119 events determined by moment tensor inversion (circles), superimposed over the shear wave velocity model (Saikia et al., 2021). The red isolines indicate the thermal structure as determined by a half-space cooling model, assuming a half-spreading rate of 16mm/yr. b) Thermal structure inverted from the shear wave velocity model shown in (a). The focal mechanism solution quality (Q1 to Q4) is indicated in the legend (dark dots are constrained better than the light ones). The horizontal blue lines denote the location of the 4 positive flower structures, whereas the vertical shaded bars indicate the seismicity gaps. Seismicity is constrained above the 600°C isotherm.

CONCLUSIONS

We investigated the seismotectonic properties along Chain TF, equatorial MAR, by combining a ~1-year microseismicity with 45-year strong event (M>5.5) occurrence and geophysical data. Our results are summarized as:

- There are three 50-100 km long active segments (asperities) separated by smaller (~15-30km long) seismic gaps (barriers).
- The lateral heterogeneity and the non-regular occurrence of large events strongly suggest highly heterogeneous and fractured damage zones, supporting either the thick seismogenic patch or the multi-mode rupture model (e.g. Boettcher and Jordan, 2004; Aderhold and Abercrombie, 2016).
- Microseismicity occurs at much higher rates at the eastern part, where negative rMBA values dominate and there is a large positive flower structure (shallower bathymetry).
- The morphology, gravity anomalies, focal mechanism solutions and magnitude distribution at the easternmost flower structure, suggest that crust may have been thickened due to transpression, and/or density could have been decreased due to serpentinization masking crustal thinning (Harmon et al., 2018).
- Areas coated with serpentinized peridotite at different degrees (negative rMBA) potentially create relatively weak barrier zones (aseismic or swarms with high b-values), whereas dry, gabbroic crust (positive rMBA) may act as an asperity region (low b-values), with such behaviour potentially demonstrating a time-dependent component (e.g. Reinen et al., 1991; Liu et al., 2012).

AUTHOR INFORMATION

Dr Konstantinos (Kostas) Leptokaropoulos (https://www.southampton.ac.uk/oes/about/staff/kl2c20.page) is a Research Fellow in Seismology at the University of Southampton (National Oceanography Centre), UK.

For more information please visit my Research Gate webpage:

https://www.researchgate.net/profile/Konstantinos-Leptokaropoulos-2
(https://www.researchgate.net/profile/Konstantinos-Leptokaropoulos-2)

and my Linkedin webpage:

https://www.linkedin.com/in/konstantinos-leptokaropoulos-391a0665/
(https://www.linkedin.com/in/konstantinos-leptokaropoulos-391a0665/)

email:K.Leptokaropoulos@soton.ac.uk

ABSTRACT

Oceanic Transform Faults (TF) comprise first order discontinuities bounded between mid-ocean ridge spreading centres. TF mainly accommodate strike slip motion, separating lithospheric plates of different age and thermal structure. Oceanic TF are intriguing in that they do not produce earthquakes as large as might be expected given their long length, with seismic slip corresponding only to a small fraction of the total tectonic slip. The relative geologic simplicity of oceanic TF means that they are an important analogue for more hazardous continental TF, with high potential for improving insights into the earthquake cycle.

We investigate the earthquake properties along Chain, a ~300 km long TF in the equatorial MAR by combining both microseismic and teleseismic data. We use the ~1-year microseismicity data (total of 812 events) gathered during the PI-LAB (Passive Imaging of the Lithosphere-Asthenosphere Boundary) experiment and EURO-LAB (Experiment to Unearth the Rheological Lithosphere-Asthenosphere Boundary). We perform cluster analysis in multi-dimensional phase space, consisting of various seismic (epicentral coordinates, magnitude) and geophysical (gravity anomalies, bathymetry, tidal height) parameters. We investigate potential triggering mechanisms, including tidal, static and dynamic stresses. We extend our analysis back in time by considering stronger earthquakes (M_W>~5.0) from Global Centroid Moment Tensor (GCMT) since 1976. We find three unique, 50-100 km long clusters or segments from our analysis going from east to west, separated by seismic gaps. Microseismic activity is highest at the eastern segment of Chain where there is the largest positive flower structure, negative rMBA gravity anomaly but very few M>5.5 events. The western segment has reduced seismicity rates relative to the eastern, and is associated with a positive rMBA and a few small flower structures. The central segment is bounded between two seismic gaps and demonstrates relatively high activity rates in the middle. Our result suggests that trans-pression of highly altered mantle/crust and/or high pore pressure due to hydrothermal fluid circulation in the eastern flower structure enhances seismic activity. Overall, we find the existence of consecutive locking and creeping segments, with some of the patches exhibiting hybrid behaviour, potentially causing their sporadic activation/reactivation.

REFERENCES

Aki, K. (1965), Maximum likelihood estimate of b in the formula logN = a - bM and its confidence limits, *Bull. Earthq. Res. Inst. Tokyo Univ.,* 43, 237–239.

Aderhold, K. & R. E. Abercrombie (2016), The 2015 Mw 7.1 earthquake on the Charlie-Gibbs transform fault: Repeating earthquakes and multimodal slip on a slow oceanic transform. *Geophys. Res. Lett.*, 43, 6119–6128.

Agnew, D. C. (1997), NLOADF: a program for computing ocean-tide loading, *J. Geophys. Res.*, 102, 5109–5110.

Amorèse D, J.-R. Grasso and Rydelek P.A. (2010), On varying b values with depth: results from computer-intensive tests for Southern California, *Geophys. J. Int.*, 180, 347–360, doi: 10.1111/j.1365-246X.2009.04414 .x.

Boettcher, M. S. & T. H. Jordan (2004), Earthquake scaling relations for mid-ocean ridge transform faults. *J. Geophys. Res.* 109, B12302.

Harmon, N., C. Rychert, M. Agius, S. Tharimena, T. Le Bas, J.M. Kendall and S. Constable, (2018), Marine geophysical investigation of the Chain Fracture Zone in the equatorial Atlantic from the PI-LAB experiment. *J. Geophys. Res. Solid Earth*, 123, 11,016–11,030, https://doi.org/10.1029/ (https://doi.org/10.1029/) 2018JB015982.

Heimann, S., M. Isken, D. Kühn, H. Sudhaus, A. Steinberg, H. Vasyura-Bathke, et al. (2018), *Grond - A probabilistic earthquake source inversion framework*. V. 1.0. Potsdam: GFZ Data Services.

Egbert, G. D. and S. Y. Erofeeva (2002), Efficient inverse modeling of barotropic ocean tides., *J. Atmos. Ocean. Technol.*, 19, 183-204.

Ekström, G., M. Nettles and A. Dziewoński (2012), The global CMT project 2004–2010: centroid-moment tensors for 13,017 earthquakes, *Phys. Earth. Planet. Int.*, 200–201, 1–9

Lasocki S. (2014), Transformation to equivalent dimension - a new methodology to study earthquake clustering, *Geophys. J. Int.*, 197, 1224-1235, doi:10.1093/gji/ggu062.

Leptokaropoulos, K. (2020), Magnitude distribution complexity and variation at The Geysers geothermal field, *Geophys. J. Int., 222*, 893-906, doi: 10.1093/gji/ggaa208 (https://doi.org/10.1093/gji/ggaa208).

Leptokaropoulos, K., A. Adamaki, R. Roberts, C. Gkarlaouni and P. Paradisopoulou (2018), Impact of magnitude uncertainties on seismic catalog properties, Geophys. J. Int., 213, 941-950, doi: 10.1093/gji/ggy023.

Leptokaropoulos, K., N. Harmon, S. Hicks, C. A. Rychert, D. Schlaphorst and J. M. Kendall (2021), Tidal Triggering of Microseismicity at the Equatorial Mid-Atlantic Ridge, Inferred from the PI-LAB experiment, *J. Geophys. Res.: Solid Earth*, 126, e2021JB022251, doi: 10.1029/2021JB022251 (https://doi.org/10.1029 /2021JB022251).

Lin, J. and R. S. Stein (2004), Stress triggering in thrust and subduction earthquakes, and stress interaction between the southern San Andreas and nearby thrust and strike-slip faults, *J. Geophys. Res.*, v. 109, B02303, doi:10.1029/2003JB002607.

Liu, Y., J. J. McGuire, & M. D. Behn (2012), Frictional behavior of oceanic transform faults and its influence on earthquake characteristics, *J. Geophys. Res.* 117, B04315.

Lomax, A., J. Virieux, P. Volant & C. Berge-Thierry (2000), Probabilistic earthquake location in 3D and layered models. *Advances in Seismic Event Location*, 18, 101– 134.

Marsaglia, G. and J. Marsaglia (2004), Evaluating the Anderson-Darling distribution, J. Stat. Soft., 9, 1-5.

Michael, A. J. (1984), Determination of stress from slip data: faults and folds, J. Geophys. Res., 89, 11,517-11,526.

Reinen, L. A., J. D. Weeks, & T. E. Tullis (1991), The frictional behavior of serpentinite: Implications for aseismic creep. *Geophys. Res. Lett.*, 18, 1921–1924.

Saikia, U., C. Rychert, N. Harmon and J. M. Kendall (2020), Sediment structure at the equatorial mid-atlantic ridge constrained by seafloor admittance using data from the PI-LAB experiment, *Mar. Geophys. Res.*, 41, 3, doi: 10.1007/s11001-020-09402-0.

Schuster, A. (1897), On lunar and solar periodicities of earthquakes, Proc. R. Soc. Lond., 61, 455–465.

Shi, P., W. Meng and R. Pockalny (2021), The ubiquitous creeping segments on oceanic transform faults, *Geology*, doi.org/10.1130/G49562.1.

Siegel, A. F. (1982), Robust regression using repeated medians, Biometrika, 69, 242–244.

Silverman, B.W. (1986), *Density Estimation for Statistics and Data Analysis*, Monograph, CRC Press, 175 pp.

Toda, S., R. S. Stein, K. Richards-Dinger and S. Bozkurt (2005), Forecasting the evolution of seismicity in southern California: Animations built on earthquake stress transfer, *J. Geophys. Res.*, v. 110, B05S16, doi:10.1029/2004JB003415.

Vavryčuk, V. (2014). Iterative joint inversion for stress and fault orientations from focal mechanisms, *Geophys. J. Int.*, 199, 69-77, doi: 10.1093/gji/ggu224.

Ward, J.H., 1963. Hierarchical grouping to optimize an objective function, *J. Am. Stat. Assoc.*, 58, 236–244.